

Entanglement measures for non-conformal D-branes

Arindam Lala*

Instituto de Física,
Pontificia Universidad Católica de Valparaíso,
Casilla 4059, Valparaíso, Chile

Abstract

We study various entanglement measures associated with certain non-conformal field theories. We consider non-conformal Dp -brane backgrounds, which are dual to these field theories, for our holographic analysis. Restricting our interests in $p = 1, 2, 4$, we explicitly compute properties of holographic entanglement entropy and entanglement wedge cross section, E_W , corresponding to two parallel strip shaped boundary subregions in these set ups. We study low and high temperature behaviours of these quantities analytically as well as using numerical methods. In all cases, the E_W decrease monotonically with temperature. We observe discontinuous jumps in E_W while the width of (as well as the separation between) the subregions reach critical values in all the cases considered. However, the corresponding holographic mutual information I_M continuously decreases to zero for the aforementioned configurations. We also notice that the conjectured inequality $E_W \geq I_M/2$ still holds for non-conformal field theories as well. We analytically determine the critical separation between these subregions that triggers a phase transition in the holographic mutual information.

1 Introduction

The Gauge/Gravity duality [1, 2, 3] has enriched our understanding of concepts related to quantum information theory. Perhaps the most prominent of all these examples is the holographic computations of entanglement entropy of the dual boundary theory of interest which is particularly useful in determining the entanglement entropy of pure states [4, 5, 6, 7, 8]. This holographic entanglement entropy (HEE) proposal presents an interpretation of the entanglement entropy of the boundary field theory in terms of a geometric quantity, namely, the minimal surface which is extended into the bulk. However, this prescription can easily be extended to the case of more than one boundary intervals [9]. In this regard, a related quantity known as the holographic mutual information (HMI), $I_M(A, B)$, between two disjoint boundary intervals A and B can be determined [9, 10, 11, 12]. Interestingly, $I_M(A, B) \geq 0$ and it is UV finite. Moreover, it undergoes a phase transition at some critical separation between the two intervals in which case the two subsystems become disentangled [9, 11].

On the other hand, in order to determine the entanglement entropy of mixed states, an interesting measure known as the holographic entanglement wedge cross section (EWCS), E_W , is of much discussion in recent times [13, 14]. It is defined to be proportional to the minimal area of the entanglement wedge constructed out of the two intervals A and B ¹. This quantity is conjectured to be

*arindam.physics1@gmail.com, arindam.lala@pucv.cl

¹The entanglement wedge is a bulk region whose boundary is given by $\partial W_{AB} = A \cup B \cup \Gamma_{AB}^m$. Here Γ_{AB}^m is the minimal surface associated with the union AB .

holographic dual to entanglement of purification (EoP) [15] which measures the correlation between A and B and, for pure states, reduces to entanglement entropy². Although this proposal still has not been fully understood, there are certain indirect tests that this conjecture has passed, such as the following inequality [15],

$$E_W \geq \frac{I_M(A, B)}{2}, \quad (1)$$

which has been proven explicitly using the holographic duality [13, 14]. Very recently, based on the formalism developed in [13, 14], various properties of EWCS along with HEE and HMI have been studied in different holographic set-ups [19, 20, 21, 22, 23, 24]³. All these examples mostly deal with conformal boundary theories in which cases the inequality (1) holds explicitly. Moreover, both E_W and HMI decrease monotonically and E_W is shown to undergo a discontinuous phase transition at high temperature.⁴

The purpose of the present paper is to extend the study of certain aspects of EWCS, HEE and HMI to non-conformal field theories which are dual to non-conformal Dp -branes [28, 29, 30, 31, 32]. This will eventually extend the formalism to the study of non-conformal field theories as well, which is presently absent in the literature. This, in turn, could enable us to explore properties of scale non-invariant field theories abundant in Nature.

The holographic correspondence between non-conformal Dp -branes and their dual field theories were studied in details in [28] where the (super)gravity description is controlled by an effective dimensionless coupling constant g_{eff} . However, in a more general set up, the 10-dimensional theory of [28] can be dimensionally reduced to obtain an effective $(p+2)$ -dimensional theory described by Einstein-dilaton gravity [29, 30, 31, 32]. Interestingly, the space-time metric obtained in the later case is found to be conformal to that of AdS_{p+2} ⁵.

In this paper, we study the EWCS of two disjoint boundary intervals in the shape of parallel strips each of width ℓ and length L . The low as well as high temperature behaviours of the EWCS are also studied. We restrict ourselves to the cases $p = 1, 2, 4$. However, results corresponding to the conformal $p = 3$ case are also provided for sake of completeness of the analyses. We also discuss the behaviours of the HEE corresponding to the thermal boundary field theory along the line of analysis of [12, 37, 38, 39]. In our analysis we observe that, in all cases the EWCS scales with the area of the entangling region contrary to the volume scaling of the HEE. In addition, it monotonically decreases to zero value for large temperatures beyond certain critical value of the separation h between the two disjoint intervals at which they become disentangled. However, in all cases, the corresponding HMI are monotonically decreasing functions as the critical separation between the strips is approached. Moreover, we also check the validity of the above inequality (1) explicitly in these set-ups.

The paper is organized as follows. In section 2 we give a brief account of the non-conformal gravity backgrounds. In section 3 we provide the computation of the EWCS and HEE corresponding to the strip shaped regions. The low and high temperature behaviours of these quantities are studied subsequently. The values of the critical distance of separation between the entangling regions are also determined by studying the corresponding HMI. We finally conclude in section 4.

²It must be mentioned that, the E_W has also been proposed to be gravity dual of holographic entanglement negativity [16] and reflected entropy [17, 18].

³Another promising direction, which is extensively based on the entanglement wedge construction, is the study of time evolution of mixed state correlation measures after global as well as local quantum quenches; see, for example, [25, 26, 27]. However, we shall not touch upon this aspect in this article.

⁴Note that, in [20] non-monotonous behaviours of HMI and EWCS have been reported, however in a different holographic set-up.

⁵Starting from [28], non-conformal brane plane wave backgrounds have also been constructed in [33, 34] which are shown to allow non-trivial hyperscaling violating backgrounds upon appropriate dimensional reduction. Also, aspects of holographic entanglement entropy have been studied within these theories; see, e.g., [35, 36].

2 The holographic set up

In this paper, we study quantum information quantities for certain non-conformal field theories. In order to do so, we consider nonconformal Dp-brane backgrounds dual to these field theories [28]. Here we first mention the corresponding constructions provided in [28] and then very briefly review a more general dimensionally reduced model following [29, 30] which we subsequently consider in all our computations.

The background generated from N coincident extremal Dp-branes in the string frame can be written as [28]

$$\begin{aligned} ds^2 &= \alpha' \left[\frac{U^{(7-p)/2}}{g_{YM} \sqrt{d_p N}} \left(-dt^2 + \sum_{i=1}^p dx_i^2 \right) + \frac{g_{YM} \sqrt{d_p N}}{U^{(7-p)/2}} dU^2 + g_{YM} \sqrt{d_p N} U^{(p-3)/2} d\Omega_{8-p}^2 \right], \\ e^\phi &= (2\pi)^{2-p} g_{YM}^2 \left(\frac{g_{YM}^2 N d_p}{U^{7-p}} \right)^{\frac{3-p}{4}}, \end{aligned} \quad (2)$$

where

$$d_p = 2^{7-p} \pi^{\frac{9-3p}{2}} \Gamma\left(\frac{7-p}{2}\right), \quad U = \frac{r}{\alpha'}, \quad (3)$$

and the limits $g_{YM}^2 \sim g_s \alpha'^{\frac{p-3}{2}} = \text{fixed}$, $U = \text{fixed}$ and $\alpha' \rightarrow 0$ have been taken. On top of that, the validity of the supergravity description is controlled by the dimensionless coupling constant $g_{eff} = g_{YM}^2 N U^{p-3}$. In the non-extremal limit the above solution (2) can be expressed as

$$\begin{aligned} ds^2 &= \alpha' \left[\frac{U^{(7-p)/2}}{g_{YM} \sqrt{d_p N}} \left(-f(U) dt^2 + \sum_{i=1}^p dx_i^2 \right) + \frac{g(U) g_{YM} \sqrt{d_p N}}{U^{(7-p)/2}} dU^2 + g_{YM} \sqrt{d_p N} U^{(p-3)/2} d\Omega_{8-p}^2 \right], \\ e^\phi &= (2\pi)^{2-p} g_{YM}^2 \left(\frac{g_{YM}^2 N d_p}{U^{7-p}} \right)^{\frac{3-p}{4}}, \end{aligned} \quad (4)$$

where

$$f(U) = 1 - \frac{U_0^{7-p}}{U^{7-p}}, \quad g(U) = \frac{1}{f(U)} \approx 1 + \frac{U_0^{7-p}}{U^{7-p}}. \quad (5)$$

However, in a more general set up, we can perform an S^{8-p} Kaluza-Klein compactification of the above string-frame metric (4) to $(p+2)$ -dimensions. The effective theory (in the Einstein frame) is then characterized by the $(p+2)$ -dimensional Einstein-Dilaton action [29, 30, 31, 32]

$$S = \frac{N^2}{16\pi G_N^{p+2}} \left[\int d^{p+2}x \sqrt{-g} \left(\mathcal{R} - \frac{1}{2} \partial_\mu \Phi \partial^\mu \Phi + V(\Phi) \right) - 2 \int d^{p+1}x \sqrt{-\gamma} \mathcal{K} \right], \quad (6)$$

where

$$V(\Phi) = \frac{1}{2} (9-p)(7-p) N^{-2\lambda/p} e^{a\Phi}, \quad \Phi = \frac{2\sqrt{2(9-p)}}{\sqrt{p}(7-p)} \phi, \quad (7)$$

$$a = -\frac{\sqrt{2}(p-3)}{\sqrt{p}(9-p)}, \quad \lambda = \frac{2(p-3)}{(7-p)}, \quad (8)$$

and \mathcal{K} , γ_{ab} are the extrinsic curvature and the induced boundary metric, respectively. Also in (6) G_N^{p+2} is the $(p+2)$ -dimensional Newton's constant. The above theory (6) allows for black brane solutions given by [29]-[32]

$$ds^2 = (Ne^\phi)^{\frac{2\lambda}{p}} \left[\frac{u^2}{\Delta^2} \left(-f(u)dt^2 + \sum_{i=1}^p dx_i^2 \right) + \frac{\Delta^2 du^2}{u^2 f(u)} \right], \quad (9a)$$

$$f(u) = 1 - \left(\frac{u_0}{u} \right)^{\frac{2(7-p)}{(5-p)}}, \quad (9b)$$

$$e^\phi = \frac{1}{N} (g_{YM}^2 N)^{\frac{7-p}{2(5-p)}} \left(\frac{u}{\Delta} \right)^{\frac{(p-7)(p-3)}{2(p-5)}}, \quad (9c)$$

$$u_0^2 = \frac{U_0^{5-p}}{(g_{YM}^2 N)}, \quad \Delta = \frac{2}{5-p}. \quad (9d)$$

Now the Hawking temperature of the Dp-brane can be computed by the usual method of analytical continuation of the metric (9a) to the Euclidean sector, $t \rightarrow i\tau$ [40]. The resulting expression for the temperature can be calculated as

$$T = \frac{1}{4\pi\Delta^2} \frac{2(p-7)}{(p-5)z_0}, \quad (10)$$

where the following change in coordinates $u \rightarrow 1/z$ and $u_0 \rightarrow 1/z_0$ has been taken into account [31, 32].

On the other hand, the thermal entropy of the Dp-branes can be computed as

$$\begin{aligned} S_{\text{th}} &= \frac{1}{4G_N^{p+2}} \int_{-\ell/2}^{\ell/2} dx \int_{-L/2}^{L/2} \prod_{i=1}^{p-1} dx_i \left(g_{xx} \prod_{i=1}^{p-1} g_{x_i x_i} \right)^{\frac{1}{2}} \\ &= \frac{L^{p-1} \ell}{4G_N^{p+2}} (g_{YM}^2 N)^{\frac{p-3}{5-p}} \left(\frac{1}{z_0 \Delta} \right)^{\frac{p-9}{p-5}}. \end{aligned} \quad (11)$$

3 Entanglement Wedge Cross Section (EWCS)

Let us consider two long parallel strips each of width ℓ and separated by a distance h . They indeed represent two subregions A and B and is shown as dark black lines in fig.1. We choose the following specific symmetric (around $x = 0$) configurations for the subsystems [19, 20, 21]:

$$A = \left\{ \frac{h}{2} < x < \ell + \frac{h}{2}; \quad -\frac{L}{2} < x_2, x_3, \dots, x_{p-1} < \frac{L}{2} \right\}, \quad (12a)$$

$$B = \left\{ -\ell - \frac{h}{2} < x < -\frac{h}{2}; \quad -\frac{L}{2} < x_2, x_3, \dots, x_{p-1} < \frac{L}{2} \right\}. \quad (12b)$$

Now the minimal surface, Γ_{AB}^m , that separates the two subsystems A and B is given by the vertical constant x surface at $x = 0$ which is a space-like slice. The induced metric on this slice can be written as

$$\begin{aligned} ds_{\Gamma_{AB}^m}^2 &= (Ne^\phi)^{\frac{2\lambda}{p}} \left[\frac{1}{z^2 \Delta^2} \sum_{i=1}^{p-1} dx_i^2 + \frac{\Delta^2 dz^2}{z^2 f(z)} \right], \\ f(z) &= 1 - \left(\frac{z}{z_0} \right)^{\frac{2(7-p)}{(5-p)}}. \end{aligned} \quad (13)$$

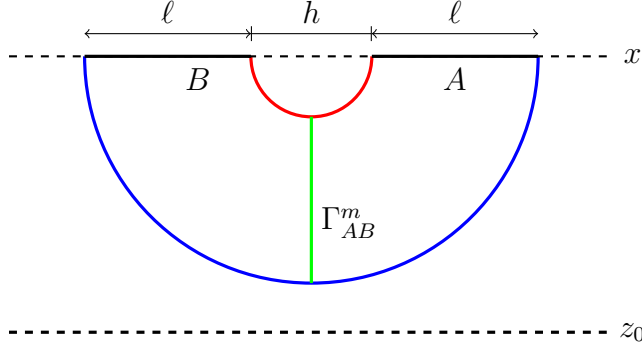


Figure 1: A schematic 2D diagram for computing entanglement wedge cross section (EWCS) Γ_{AB}^m . Here we consider two parallel strips each of width ℓ separated by h . Here z_0 represents the horizon of the brane.

Next, we use the general expression for the entanglement wedge cross section (EWCS) corresponding to the two subregions A and B given by [13, 14, 19, 20, 21]

$$E_W = \frac{\text{Area}(\Gamma_{AB}^m)}{4G_{\text{N}}^{p+2}}. \quad (14)$$

Using (13) and (14) we finally obtain⁶

$$\begin{aligned} E_W &= \frac{L^{p-1}(g_{YM}^2 N)^{\frac{p-3}{5-p}}}{4G_{\text{N}}^{p+2}\Delta^{\frac{p-1}{5-p}}} \int_{z_t(h)}^{z_t(2\ell+h)} dz \frac{z^{\frac{9-p}{p-5}}}{\sqrt{f(z)}} \\ &= \frac{L^{p-1}(g_{YM}^2 N)^{\frac{p-3}{5-p}}}{4G_{\text{N}}^{p+2}\Delta^{\frac{p-1}{5-p}}} \sum_{n=0}^{\infty} \frac{\Gamma(n+\frac{1}{2})(p-5)}{\sqrt{\pi}(4+2n(p-7))\Gamma(n+1)} \left(\frac{z_t(2\ell+h)^\delta}{z_0^{n\alpha}} - \frac{z_t(h)^\delta}{z_0^{n\alpha}} \right), \end{aligned} \quad (15)$$

where we have denoted

$$\alpha = \frac{2(7-p)}{(5-p)}, \quad \delta = \frac{4+2n(p-7)}{(p-5)}. \quad (16)$$

We now use the Ryu-Tagayanagi prescription [4, 5] in order to find the holographic entanglement entropy (HEE) corresponding to a strip shaped region in the boundary of the geometry (9a) which can be expressed as [37]

$$S_{\text{EE}} = \frac{\mathcal{A}_\gamma}{4G_{\text{N}}^{p+2}}, \quad (17)$$

where \mathcal{A}_γ is the area of the p -dimensional Ryu-Takayanagi surface γ .

In our analysis, we choose the strip parametrized as

$$-\frac{\ell}{2} \leq x \leq \frac{\ell}{2}, \quad -\frac{L}{2} \leq x_2, \dots, x_{p-1} \leq \frac{L}{2}. \quad (18)$$

Thus the HEE functional can be written as

$$S_{\text{EE}} = \frac{L^{p-1}}{2G_{\text{N}}^{p+2}} (g_{YM}^2 N)^{\frac{p-3}{5-p}} \Delta^{\frac{9-p}{p-5}} \int dz z^{\frac{9-p}{p-5}} \sqrt{x'^2 + \frac{\Delta^4}{f(z)}}. \quad (19)$$

⁶Notice that the integration in (15) can be evaluated exactly; however, we find it convenient to express it in the series form [12, 38].

Interestingly, the above functional (19) has no explicit dependence on $x(z)$, and hence we can find the following first integral of motion by applying the conservation of energy of the system,

$$x'(z) = \pm \frac{\Delta^2}{\sqrt{f(z) \left(\left(\frac{z}{z_t} \right)^{2 \frac{(9-p)}{(p-5)}} - 1 \right)}}, \quad (20)$$

where z_t is the turning point of the minimal surface. Also note that, in deriving (20) we have used the boundary condition $\lim_{x \rightarrow \infty} z = z_t$.

In the next step, we integrate (20) to obtain a relation between strip width ℓ and the turning point z_t as

$$\ell = 2\Delta^2 z_t \int_0^1 dv \frac{v^{\frac{9-p}{5-p}}}{\sqrt{f(v)} \sqrt{1 - v^{2 \frac{(9-p)}{(5-p)}}}}, \quad (21)$$

where we have defined $v = \frac{z}{z_t}$ and considered the fact that $1 \leq p \leq 4$.

Substituting (20) into (19) we finally obtain

$$S_{\text{EE}} = \frac{L^{p-1}}{2G_{\text{N}}^{p+2}} (g_{YM}^2 N)^{\frac{p-3}{5-p}} \frac{\Delta^{\frac{p-1}{5-p}}}{z_t^{\frac{4}{5-p}}} \int_0^1 \frac{dv}{v^{\frac{9-p}{5-p}}} \frac{1}{\sqrt{f(v) \left(1 - v^{2 \frac{(9-p)}{(5-p)}} \right)}}. \quad (22)$$

The integrations appearing in the above equations (21) and (22) can be evaluated easily; and hence the width and the HEE can respectively be expressed as [12, 38]

$$\ell = \Delta^2 z_t \sum_{n=0}^{\infty} \frac{\Gamma(n + \frac{1}{2}) \Gamma\left(\frac{(n+1)(p-7)}{p-9}\right)}{\Gamma(n+1) \Gamma\left(\frac{3}{2} + n + \frac{2(n+1)}{(p-9)}\right)} \frac{(p-5)}{(p-9)} \left(\frac{z_t}{z_0}\right)^{2n \frac{(7-p)}{(5-p)}}, \quad (23)$$

$$S_{\text{EE}} = S_{\text{sin}} + \frac{L^{p-1}}{2G_{\text{N}}^{p+2}} (g_{YM}^2 N)^{\frac{p-3}{5-p}} \frac{\Delta^{\frac{p-1}{5-p}}}{z_t^{\frac{4}{5-p}}} \left[\frac{\sqrt{\pi}(p-5) \Gamma\left(\frac{2}{p-9}\right)}{2(p-9) \Gamma\left(\frac{p-5}{2(p-9)}\right)} + \sum_{n=1}^{\infty} \frac{\Gamma(n + \frac{1}{2}) \Gamma\left(n + \frac{2(n+1)}{p-9}\right)}{\Gamma(n+1) \Gamma\left(\frac{p-5+2n(p-7)}{2(p-9)}\right)} \frac{(p-5)}{2(p-9)} \left(\frac{z_t}{z_0}\right)^{2n \frac{(7-p)}{(5-p)}} \right], \quad (24)$$

where the singular part of the HEE can be written as

$$S_{\text{sin}} = \frac{L^{p-1}}{2G_{\text{N}}^{p+2}} (g_{YM}^2 N)^{\frac{p-3}{5-p}} \frac{\Delta^{\frac{p-1}{5-p}}}{\epsilon^{\frac{4}{5-p}}} \left(\frac{5-p}{4} \right). \quad (25)$$

Notice that, in (25) ϵ is the ultraviolet (UV) cut-off.

At this point of discussion, note that, we can get the expressions for E_W as well as S_{EE} corresponding to the conformal (D3-brane) case by substituting $p = 3$ in (15) and (22), respectively. In the next sections we also compute the corresponding expressions for D3-branes for completeness of the analysis which indeed match with those already exist in the literature; see, e.g., [5, 9, 19, 20, 21, 38, 39]. In addition, we shall also study the corresponding quantities by plotting their behaviours numerically.

In our numerical analysis, we shall set the pre factor $\frac{L^{p-1}}{4G_{\text{N}}^{p+2}} \frac{(g_{YM}^2 N)^{\frac{(p-3)}{(5-p)}}}{\Delta^{\frac{p-1}{5-p}}} = 1$.

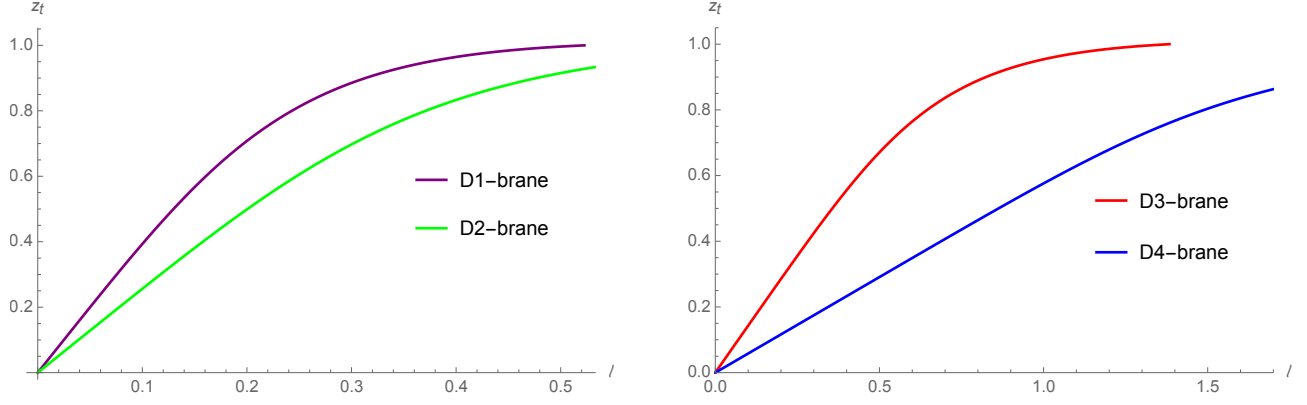


Figure 2: z_t vs. ℓ plot for different Dp -brane backgrounds. The turning point vanishes at $\ell = 0$, and as ℓ increases, z_t approaches 1. Here we set the horizon radius $z_0 = 1$.

3.1 Low and high temperature behaviours of the HEE

In this section, we study both the low and high temperature behaviours of the holographic entanglement entropy (HEE) (24) in the backgrounds (9a). In order to achieve this analytically, we need to solve the turning point z_t in terms of the subregion length ℓ . It is evident from (23) that this procedure can only be applied in the low and high temperature limits.

The low temperature limit is geometrically realized when the turning point z_t corresponding to the RT surface(s) lies far away from the horizon z_0 of the black brane in the deep interior of the bulk: $z_t \ll z_0$. On the other hand, for the considered range of values of p , $1 \leq p \leq 4$, the exponent $\frac{(7-p)}{(5-p)} \leq 3$. Hence, it is sufficient to keep terms upto order $\mathcal{O}\left(4^{\frac{(7-p)}{(5-p)}}\right)$ in the perturbative expansion. Thus the resulting expression for the turning point in (23) may be written as

$$z_t \approx \frac{\ell}{\Delta^2 \Upsilon} \left[1 - \frac{\sqrt{\pi}(p-5)\Gamma\left(\frac{2(p-7)}{p-9}\right)}{2(p-9)\Gamma\left(\frac{5}{2} + \frac{4}{p-9}\right)} \frac{1}{\Upsilon} \left(\frac{\ell}{\Delta^2 z_0 \Upsilon}\right)^{\frac{2(7-p)}{(5-p)}} + \left\{ \left(\frac{\sqrt{\pi}(p-5)\Gamma\left(\frac{2(p-7)}{p-9}\right)}{2(p-9)\Gamma\left(\frac{5}{2} + \frac{4}{p-9}\right)} \frac{1}{\Upsilon}\right)^2 - \left(\frac{3\sqrt{\pi}(p-5)}{8(p-9)} \frac{\Gamma\left(\frac{3(p-7)}{(p-9)}\right)}{\Gamma\left(\frac{7}{2} + \frac{6}{p-9}\right)} \frac{1}{\Upsilon}\right) \right\} \left(\frac{\ell}{\Delta^2 z_0 \Upsilon}\right)^{\frac{4(7-p)}{(5-p)}} + \mathcal{O}\left(\frac{\ell}{\Delta^2 z_0 \Upsilon}\right)^{\frac{6(7-p)}{(5-p)}} \right], \quad (26)$$

where we have defined

$$\Upsilon = \frac{\sqrt{\pi}(p-5) \Gamma\left(\frac{p-7}{p-9}\right)}{(p-9) \Gamma\left(\frac{3}{2} + \frac{2}{p-9}\right)}. \quad (27)$$

With this approximation and substituting (26) into (24), the final expressions for the HEE at low temperatures can be written as follows.⁷

D1-brane

$$S_{\text{EE}LT}^{(D1)} = \bar{C}_1 \left[S_0 + \mathcal{C}_1 \left(\frac{1}{\ell}\right) \left(1 + \mathcal{C}_2 \left(\frac{\pi T \ell}{3}\right)^3 + \mathcal{C}_3 \left(\frac{\pi T \ell}{3}\right)^6 + \mathcal{O}(\pi T \ell / 3)^7 \right) \right], \quad (28)$$

⁷Here and what follows, the subscripts ‘LT’ and ‘HT’ denote Low Temperature and High Temperature, respectively.

where we have denoted

$$\bar{\mathcal{C}}_1 = \frac{(g_{YM}^2 N)^{-\frac{1}{2}}}{4G_N^3}, \quad S_0 = \frac{2}{\epsilon}, \quad (29)$$

and the other *constants* \mathcal{C}_1 , \mathcal{C}_2 and \mathcal{C}_3 are constants. We have explicitly written down the forms of these constants and those that appear below (\mathcal{D}_i , \mathcal{B}_i and \mathcal{E}_i , $i = 1, 2, 3$) in appendix [A](#).

D2-brane

$$S_{\text{EE}LT}^{(D2)} = \bar{\mathcal{C}}_2 \left[S_0 + \mathcal{D}_1 \left(\frac{1}{\ell} \right)^{4/3} \left(1 + \mathcal{D}_2 \left(\frac{8\pi T \ell}{15} \right)^{10/3} + \mathcal{D}_3 \left(\frac{8\pi T \ell}{15} \right)^{20/3} + \mathcal{O}(8\pi T \ell / 15)^{19/3} \right) \right], \quad (30)$$

where

$$\bar{\mathcal{C}}_2 = \frac{L(g_{YM}^2 N)^{-\frac{1}{3}}}{4G_N^4 \Delta^{\frac{1}{3}}}, \quad S_0 = \left(\frac{3}{2} \right) \left(\frac{1}{\epsilon} \right)^{4/3}, \quad (31)$$

and \mathcal{D}_1 , \mathcal{D}_2 and \mathcal{D}_3 are constants.

D3-brane[\[5, 9, 19, 20, 21, 38, 39\]](#)

$$S_{\text{EE}LT}^{(D3)} = \bar{\mathcal{C}}_3 \left[S_0 + \mathcal{B}_1 \left(\frac{1}{\ell} \right)^2 \left(1 + \mathcal{B}_2 (\pi T \ell)^4 + \mathcal{B}_3 (\pi T \ell)^8 + \mathcal{O}(\pi T \ell)^{10} \right) \right], \quad (32)$$

where

$$\bar{\mathcal{C}}_3 = \frac{L^2}{4G_N^5}, \quad S_0 = \frac{1}{\epsilon^2}, \quad (33)$$

and \mathcal{B}_1 , \mathcal{B}_2 and \mathcal{B}_3 are constants.

D4-brane

$$S_{\text{EE}LT}^{(D4)} = \bar{\mathcal{C}}_4 \left[S_0 + \mathcal{E}_1 \left(\frac{1}{\ell} \right)^4 \left(1 + \mathcal{E}_2 \left(\frac{8\pi T \ell}{3} \right)^6 + \mathcal{E}_3 \left(\frac{8\pi T \ell}{3} \right)^{12} + \mathcal{O}(8\pi T \ell / 3)^{18} \right) \right], \quad (34)$$

with

$$\bar{\mathcal{C}}_4 = \frac{L^3(g_{YM}^2 N)}{4G_N^6 \Delta^3}, \quad S_0 = \left(\frac{1}{2} \right) \left(\frac{1}{\epsilon} \right)^4, \quad (35)$$

and \mathcal{E}_1 , \mathcal{E}_2 and \mathcal{E}_3 are constants.

Notice that, when the temperature is zero ($T = 0$), the leading order finite terms appearing in [\(28\)](#), [\(30\)](#), [\(32\)](#) and [\(34\)](#) agree with those prescribed in [\[37\]](#).

On the other hand, at high temperatures the turning point z_t approaches the horizon of the black branes, $z_t \rightarrow z_0$, and indeed wraps a part of the horizon. Thus the leading contribution comes from

the near horizon part of the surface. On top of that, the entire bulk geometry contributes in the form of subleading terms [12, 38]. The following combination is found to be converging as the limit $z_t \rightarrow z_0$ is taken and hence we proceed our analysis with this combination [12, 21, 38].

$$S_{\text{EE}} - \frac{L^{p-1}(g_{YM}^2 N)^{\frac{p-3}{5-p}}}{4G_N^{p+2}} \left(\frac{1}{\Delta z_t} \right)^{\frac{9-p}{5-p}} \ell = \frac{L^{p-1}(g_{YM}^2 N)^{\frac{p-3}{5-p}}}{2G_N^{p+2} \Delta^{\frac{p-1}{5-p}}} \left(\frac{1}{z_t} \right)^{\frac{4}{5-p}} \int_{\epsilon/z_t}^1 dv \frac{\sqrt{1-v^{\frac{2(9-p)}{5-p}}}}{\sqrt{f(v)} v^{\frac{9-p}{5-p}}}. \quad (36)$$

Using (36) we can now recast the finite part of the HEE as

$$S_{\text{EE}} = \frac{L^{p-1}(g_{YM}^2 N)^{\frac{p-3}{5-p}}}{4G_N^{p+2}} \left(\frac{1}{\Delta z_t} \right)^{\frac{9-p}{5-p}} \ell + \frac{L^{p-1}(g_{YM}^2 N)^{\frac{p-3}{5-p}}}{2G_N^{p+2} \Delta^{\frac{p-1}{5-p}}} \left(\frac{1}{z_t} \right)^{\frac{4}{5-p}} \left[\frac{(p-5)}{4} {}_2F_1 \left(\frac{1}{2}, \frac{2}{p-9}; \frac{p-7}{p-9}; 1 \right) + \int_0^1 dv \left(\frac{\sqrt{1-v^{\frac{2(9-p)}{5-p}}}}{\sqrt{f(v)} v^{\frac{9-p}{5-p}}} - \frac{1}{v^{\frac{9-p}{5-p}} \sqrt{1-v^{\frac{2(9-p)}{5-p}}}} \right) \right], \quad (37)$$

where ${}_2F_1(a, b; c; z)$ is the usual hypergeometric function.

Finally, considering the limit $z_t \rightarrow z_0$, we can read off the expression for the HEE at high temperatures from (37) as [12, 38]

$$S_{\text{EE}_{HT}} = S_{\text{sin}} + \frac{V(g_{YM}^2 N)^{\frac{p-3}{5-p}}}{4G_N^{p+2} \Delta^{\frac{9-p}{5-p}}} \left(\frac{2\pi \Delta^2 (p-5)}{(p-7)} T \right)^{\frac{9-p}{5-p}} \left\{ 1 + 2 \left(\frac{(p-7)}{2\pi \ell T (p-5)} \right) \Theta \right\}, \quad (38)$$

where S_{sin} is the singular part of the HEE given by (25) and

$$\Theta = \frac{\sqrt{\pi}(p-5)}{(p-9)} \left[\frac{\Gamma\left(\frac{2}{p-9}\right)}{2\Gamma\left(\frac{p-5}{2(p-9)}\right)} - \frac{\Gamma\left(\frac{p-7}{p-9}\right)}{\Gamma\left(\frac{3}{2} + \frac{2}{(p-9)}\right)} \right] + \sum_{n=1}^{\infty} \frac{(p-5)\Gamma(n+\frac{1}{2})}{(p-9)\Gamma(n+1)} \left[\frac{\Gamma\left(n+\frac{2(n+1)}{p-9}\right)}{2\Gamma\left(\frac{p-5+2n(p-7)}{2(p-9)}\right)} - \frac{\Gamma\left(\frac{(n+1)(p-7)}{p-9}\right)}{\Gamma\left(\frac{3}{2} + n + \frac{2(n+1)}{(p-9)}\right)} \right]. \quad (39)$$

Note that, the finite term of the HEE in (38) scales as the volume of the entangling region $V = \ell L^{p-1}$. Also, this term is proportional to the thermal entropy (11). This is expected since at high temperature regime the contributions to the HEE of the thermal boundary field theory comes from the thermal fluctuations. Furthermore, when $p = 3$ the HEE at high temperature, (38), corresponds to the conformal case as discussed in [5, 9, 19, 20, 21, 38, 39].

3.2 Low and high temperature behaviours of the EWCS

In order to study the low and high temperature behaviours of the EWCS, we first notice that we can achieve this by taking into account the following three intrinsic scales associated with the theory: the separation distance h between the two entangling regions, the width ℓ of each of the regions and the temperature T of the boundary theory [12, 19, 20, 21, 38]. Subsequently, in this case the low temperature limit corresponds to $hT \ll \ell T \ll 1$. Note that, this corresponds to considering the temperature smaller than both the length scales associated with h and ℓ . On the other hand, the high temperature limit may be defined by considering the following inequality $hT \ll 1 \ll \ell T$

in which case the temperature is large compared to the scale associated with ℓ but small compared to that associated with h .⁸ Interestingly, this high temperature limit further amounts to taking the following two approximations: $z_t(h) \ll z_0$ and $z_t(2\ell + h) \rightarrow z_0$. The first approximation amounts to considering only the leading order term in the second term within the braces in (15), while in order the second approximation to be valid we must ensure the convergence of the first sum in (15). It is trivial to check that this is indeed the case. Thus it is safe to consider the limit $z_t(2\ell + h) \rightarrow z_0$.

Let us now discuss the different cases corresponding to $p = 1, 2, 4$ separately which correspond to D1-, D2- and D4-branes, respectively. We have also provided the corresponding expressions for D3-branes (see, e.g., [19, 20, 21]) for completeness.

D1-brane

In the low temperature limit $hT \ll \ell T \ll 1$ the EWCS (15) for the D1-branes can be computed as

$$\begin{aligned} E_{W_{LT}}^{(D1)} &= \frac{(g_{YM}^2 N)^{-\frac{1}{2}}}{4G_N^3} \sum_{n=0}^{\infty} \frac{\Gamma(n + \frac{1}{2})}{\sqrt{\pi}\Gamma(n+1)} \left(\frac{z_t(2\ell + h)^{3n-1} - z_t(h)^{3n-1}}{3n-1} \right) \cdot \frac{1}{z_0^{3n}} \\ &= \frac{(g_{YM}^2 N)^{-\frac{1}{2}}}{4G_N^3} \left[\frac{\sqrt{\pi}\Gamma(\frac{3}{4})}{8\Gamma(\frac{5}{4})} \left(\frac{1}{h} - \frac{1}{2\ell + h} \right) + \frac{64\Gamma(\frac{5}{4})^2}{\pi\Gamma(\frac{3}{4})^2} \left(1 - \frac{\sqrt{\pi}\Gamma(\frac{5}{4})}{\Gamma(\frac{3}{4})} \right) \ell(\ell + h) \left(\frac{\pi T}{3} \right)^3 + \dots \right], \end{aligned} \quad (40)$$

where we have used (10) and (26).

On the other hand, considering the aforementioned high temperature limits the behaviour of the EWCS can be determined as

$$E_{W_{HT}}^{(D1)} \approx \frac{(g_{YM}^2 N)^{-\frac{1}{2}}}{4G_N^3} T \left[\frac{\pi\tilde{\mathcal{C}}_1}{3} + \frac{\sqrt{\pi}\Gamma(\frac{3}{4})}{8\Gamma(\frac{5}{4})} \left(\frac{1}{hT} \right) + \frac{16\pi^{\frac{5}{2}}}{27} \left(\frac{\Gamma(\frac{5}{4})}{\Gamma(\frac{3}{4})} \right)^3 (hT)^2 \right], \quad (41)$$

where we have defined $\tilde{\mathcal{C}}_1 = \sum_{n=0}^{\infty} \frac{\Gamma(n + \frac{1}{2})}{\sqrt{\pi}(3n-1)\Gamma(n+1)}$.

D2-brane

In a similar manner, the low temperature behaviour of EWCS for the D2-branes (15) can be determined as

$$\begin{aligned} E_{W_{LT}}^{(D2)} &= \frac{L(g_{YM}^2 N)^{-\frac{1}{3}}}{4G_N^4 \Delta^{\frac{1}{3}}} \sum_{n=0}^{\infty} \frac{\Gamma(n + \frac{1}{2})}{\sqrt{\pi}\Gamma(n+1)} \left(\frac{z_t(2\ell + h)^{\frac{10n-4}{3}} - z_t(h)^{\frac{10n-4}{3}}}{10n-4} \right) \cdot \frac{3}{z_0^{\frac{10}{3}n}} \\ &= \frac{L(g_{YM}^2 N)^{-\frac{1}{3}}}{4G_N^4 \Delta^{\frac{1}{3}}} \left[\frac{3(2\pi)^{\frac{2}{3}}}{(21)^{\frac{4}{3}}} \left(\frac{\Gamma(\frac{5}{7})}{\Gamma(\frac{17}{14})} \right)^{\frac{4}{3}} \left(\frac{1}{h^{\frac{4}{3}}} - \frac{1}{(2\ell + h)^{\frac{4}{3}}} \right) \right. \\ &\quad \left. + \frac{441}{16\pi} \frac{\Gamma(\frac{17}{14})^2}{\Gamma(\frac{5}{7})^2} \ell(\ell + h) \left(1 - \frac{2\Gamma(\frac{17}{14})\Gamma(\frac{10}{7})}{\Gamma(\frac{5}{7})\Gamma(\frac{27}{14})} \right) \left(\frac{8\pi T}{15} \right)^{\frac{10}{3}} + \dots \right]. \end{aligned} \quad (42)$$

⁸In our calculations we shall *not* take into account another limit $\ell T \ll hT$ or $1 \ll \ell T$, $1 \ll hT$ as this corresponds to the disentangling phase of the two subregions [12, 19, 21, 38, 39].

On the other hand, at high temperature the corresponding EWCS behaves as

$$E_{W_{HT}}^{(D2)} \approx \frac{L(g_{YM}^2 N)^{-\frac{1}{3}}}{4G_N^4 \Delta^{\frac{1}{3}}} T^{\frac{4}{3}} \left[\tilde{C}_2 \left(\frac{8\pi}{15} \right)^{\frac{4}{3}} + \frac{3(2\pi)^{\frac{2}{3}}}{21^{\frac{4}{3}}} \left(\frac{\Gamma(\frac{5}{7})}{\Gamma(\frac{17}{14})} \right)^{\frac{4}{3}} \left(\frac{1}{hT} \right)^{\frac{4}{3}} \right. \\ \left. + \frac{441}{32\pi} \frac{\Gamma(\frac{17}{14})^3 \Gamma(\frac{10}{7})}{\Gamma(\frac{5}{7})^3 \Gamma(\frac{27}{14})} \left(\frac{8\pi}{15} \right)^{\frac{10}{3}} (hT)^2 \right], \quad (43)$$

$$\text{with } \tilde{C}_2 = \sum_{n=0}^{\infty} \frac{3\Gamma(n + \frac{1}{2})}{\sqrt{\pi}(10n - 4)\Gamma(n + 1)}.$$

D3-brane [19, 20, 21]

The low temperature behaviour of EWCS for the D3-branes (15) can be expressed as

$$E_{W_{LT}}^{(D3)} = \frac{L^2}{4G_N^5} \sum_{n=0}^{\infty} \frac{\Gamma(n + \frac{1}{2})}{2\sqrt{\pi}\Gamma(n + 1)} \left(\frac{z_t(2\ell + h)^{2(2n-1)} - z_t(h)^{2(2n-1)}}{2n - 1} \right) \cdot \frac{1}{z_0^{4n}} \\ = \frac{L^2}{4G_N^5} \left[\frac{2\pi\Gamma(\frac{2}{3})^2}{\Gamma(\frac{1}{6})^2} \left(\frac{1}{h^2} - \frac{1}{(2\ell + h)^2} \right) \right. \\ \left. + \frac{9\Gamma(\frac{7}{6})^2}{\pi\Gamma(\frac{2}{3})^2} \ell(\ell + h) \left(1 - \frac{2\Gamma(\frac{7}{6})\Gamma(\frac{4}{3})}{\Gamma(\frac{2}{3})\Gamma(\frac{11}{6})} \right) (\pi T)^4 + \dots \right]. \quad (44)$$

On the other hand, at high temperature the corresponding EWCS behaves as

$$E_{W_{HT}}^{(D3)} \approx \frac{L^2}{4G_N^5} T^2 \left[\tilde{C}_3 \pi^2 + \frac{4\pi\Gamma(\frac{2}{3})^2}{\Gamma(\frac{1}{6})^2} \left(\frac{1}{hT} \right)^2 + \frac{9\pi^3\Gamma(\frac{7}{6})^3\Gamma(\frac{4}{3})}{\Gamma(\frac{2}{3})^3\Gamma(\frac{11}{6})} (hT)^2 \right], \quad (45)$$

$$\text{with } \tilde{C}_3 = \sum_{n=0}^{\infty} \frac{\Gamma(n + \frac{1}{2})}{2\sqrt{\pi}(2n - 1)\Gamma(n + 1)}.$$

D4-brane

Similar to previous three cases, the low temperature behaviour of EWCS (15) corresponding to the D4-brane is given by

$$E_{W_{LT}}^{(D4)} = \frac{2L^3(g_{YM}^2 N)}{G_N^6} \sum_{n=0}^{\infty} \frac{\Gamma(n + \frac{1}{2})}{\sqrt{\pi}\Gamma(n + 1)} \left(\frac{z_t(2\ell + h)^{6n-4} - z_t(h)^{6n-4}}{6n - 4} \right) \cdot \frac{1}{z_0^{6n}} \\ = \frac{2L^3(g_{YM}^2 N)}{G_N^6} \left[\frac{1028\pi^2\Gamma(\frac{3}{5})^4}{\Gamma(\frac{1}{10})^4} \left(\frac{1}{h^4} - \frac{1}{(2\ell + h)^4} \right) \right. \\ \left. + \frac{25}{16\pi} \frac{\Gamma(\frac{11}{10})^2}{\Gamma(\frac{3}{5})^2} \left(1 - \frac{2\Gamma(\frac{11}{10})\Gamma(\frac{6}{5})}{\Gamma(\frac{3}{5})\Gamma(\frac{17}{10})} \right) \ell(\ell + h) \left(\frac{8\pi T}{3} \right)^6 + \dots \right]. \quad (46)$$

Also, at high temperature the corresponding EWCS behaves as

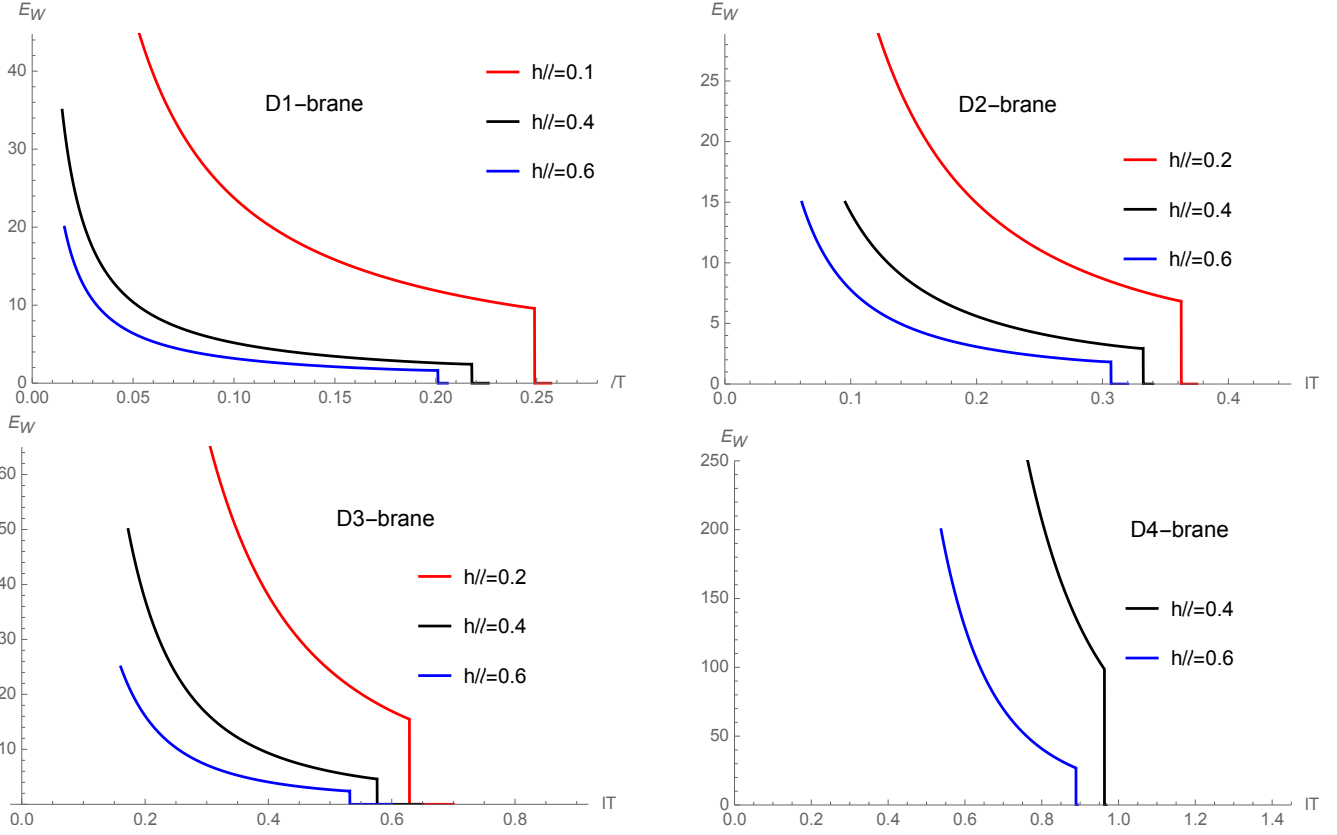


Figure 3: E_W vs. ℓT plots for different values of the dimensionless quantity h/ℓ . We have set the pre factor $\frac{L^{p-1} (g_{YM}^2 N)^{\frac{(p-3)}{(5-p)}}}{4G_N^{p+2} \Delta^{\frac{p-1}{5-p}}} = 1$. Clearly, as the temperatures ($\ell = 1$) increase E_W shows a decreasing behaviour. In all cases, the E_W sharply drops down to zero at some critical value of ℓ . The behaviour of E_W corresponding to the conformal D3-brane is also shown.

$$E_{W_{HT}}^{(D4)} \approx \frac{L^3 (g_{YM}^2 N)}{4G_N^6 \Delta^3} T^4 \left[\tilde{C}_4 \left(\frac{8\pi}{3} \right)^4 + \frac{1024\pi^2 \Gamma(\frac{3}{5})^4}{\Gamma(\frac{1}{10})^4} \left(\frac{1}{hT} \right)^4 + \frac{25}{32\pi} \frac{\Gamma(\frac{11}{10})^3 \Gamma(\frac{6}{5})}{\Gamma(\frac{3}{5})^3 \Gamma(\frac{17}{10})} \left(\frac{8\pi}{3} \right)^6 (hT)^2 \right], \quad (47)$$

$$\text{where } \tilde{C}_4 = \sum_{n=0}^{\infty} \frac{\Gamma(n + \frac{1}{2})}{\sqrt{\pi} (6n - 4) \Gamma(n + 1)}.$$

Notice that, we can numerically integrate the integration appearing in (15) for given values of p exactly. In fig.(3) and fig.(4) we plot numerically the behaviour of E_W for different values of the ratio h/ℓ for different Dp-brane backgrounds.

Let us now discuss the following observations that we can make from the low as well as high temperature behaviours of the EWCS derived above. These are listed as follows:

- When the widths of the subsystems (ℓ) are small EWCS increase sharply (fig.3). On the other hand, for a given value of the ratio h/ℓ , it converges to a finite value as ℓ increases. Also, beyond certain values of the width it sharply drops down to zero value indicating a phase transition due to the disentanglement of the subsystems. For the intermediate values of ℓ , the decrease in EWCS is monotonic.

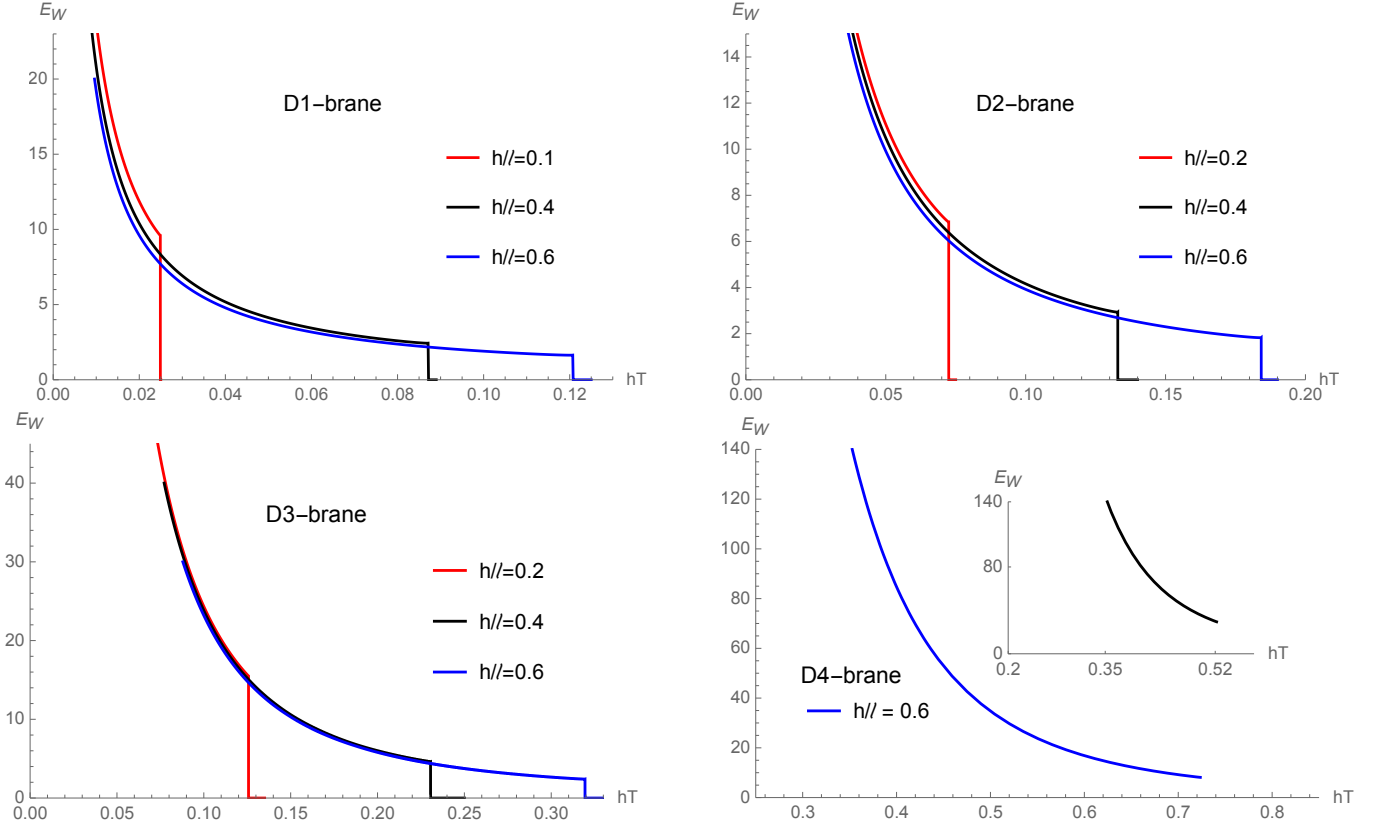


Figure 4: E_W vs. hT plots for different values of the dimensionless quantity h/ℓ . Here we have set $\frac{L^{p-1}}{4G_N^{p+2}} \frac{(g_{YM}^2 N)^{\frac{(p-3)}{(5-p)}}}{\Delta^{\frac{p-1}{5-p}}} = 1$. For clarity, the plot corresponding to $h/\ell = 0.4$ for the D4-brane is given in the inset. In all cases, the E_W jumps discontinuously to zero at some critical value of h . The plot corresponding to the conformal D3-brane is also given for comparison.

- At low temperatures, the first terms of the EWCS in (40), (42), (44) and (46) increase as the separation h between the two entangling regions decrease. Moreover, as $h \rightarrow 0$ the EWCS diverge. This is clearly visible from fig.4. Also, if we keep the width and separation between the two subregions fixed and increase the temperature, the EWCS decreases monotonically to zero ($E_W = 0$) in all cases indicating a phase transition resulting due to the disentanglement of the Ryu-Takayanagi surfaces.
- The first terms in (41), (43), (45) and (47) is proportional to the area of the entangling region, L^{p-1} . This suggests that at finite temperature the EWCS obeys an area law. This is in sharp contrast to the HEE at high temperature obtained in (38) where it scales with the volume. Similar observations have in fact been made earlier [19, 20, 21]. Moreover, this area law scaling implies that the EWCS carries more information than the HEE regarding the correlation between A and B [10, 11, 12, 19, 20, 21].

3.3 Critical separation between the strips

In this section, we determine the critical separation between the parallel strips A and B at which these two subregions become completely disentangled. This can indeed be found by calculating the holographic mutual information (HMI) between A and B [9, 10, 11, 12]. The HMI between the two

subregions A and B can be expressed as [9, 10, 11, 12, 19, 20, 21]

$$\mathbf{I}_M(\ell, h) = 2S(\ell) - S(h) - S(2\ell + h). \quad (48)$$

It measures the total correlations between A and B .

At the critical value of the separation, h_c , at which the two subregions are no longer entangled, we have

$$\mathbf{I}_M(\ell, h_c) = 0. \quad (49)$$

This is reminiscent of a first order phase transition which occurs due to the competition between different configurations for calculating $S(2\ell + h)$: when the separation distance is small the connected configuration (S_{con}) is preferred over the disconnected (S_{dis}) one. On the other hand, for large separation the disconnected configuration is preferred resulting the vanishing of the HMI [9, 11, 19]. This type of phase transitions occur for large values of the subsystem size $\ell \rightarrow \infty$. Thus $S(\ell)$ and $S(2\ell + h)$ are represented by the IR (high temperature) expression for the HEE while $S(h)$ is represented by the UV (low temperature) expression for the HEE [13, 14, 19, 20, 21].

Before proceeding to the finite temperature analysis, we notice that in the limit $\ell T \rightarrow 0$, i.e., very close to zero temperature, one can calculate the critical values of the ratio $\chi = h/\ell$ from the leading finite terms of (28), (30), (32) and (34). In order to do that, we note that in the disconnected phase the expression for HEE may be written as [9]

$$S_{\text{dis}} = 2S(\ell), \quad (50)$$

whereas, for the connected phase

$$S_{\text{con}} = S(h) + S(2\ell + h). \quad (51)$$

Now, along the transition lines $\chi_c = \text{constant}$, $S_{\text{dis}} = S_{\text{con}}$. This allows us to write the corresponding equations for χ_c as [9]

$$2 = \begin{cases} \frac{1}{\chi_c} + \frac{1}{(2+\chi_c)} & \text{for D1-brane,} \\ \frac{1}{\chi_c^{4/3}} + \frac{1}{(2+\chi_c)^{4/3}} & \text{for D2-brane,} \\ \frac{1}{\chi_c^2} + \frac{1}{(2+\chi_c)^2} & \text{for D3-brane,} \\ \frac{1}{\chi_c^4} + \frac{1}{(2+\chi_c)^4} & \text{for D4-brane.} \end{cases} \quad (52)$$

From (52) we can compute the critical values as $\chi_c = 0.618034, 0.663183, 0.732051, 0.842514$ for D1-, D2-, D3-, D4-brane, respectively. We also observe that, as p increases, the slope of the corresponding critical line also increases.

In fig.5A, we have shown the phase diagrams corresponding to the Dp -branes. Whereas, in fig.5B the behaviour of the mutual information (\mathbf{I}_M) has been shown for D2-brane. Similar plots can be drawn for other backgrounds as well. Notice that, as long as $\chi < \chi_c$ ($\chi_c = 0.663183$ for D2-brane [9]), \mathbf{I}_M is a monotonically decreasing function of ℓ ; while at χ_c it vanishes. Similar behaviours of \mathbf{I}_M were observed for pure AdS_{d+1} backgrounds in [20]. Also note that, in plotting fig.5B numerically we have used (37) and (48).

We now move on to the finite temperature cases and compute the critical separation, h_c . However, due to the complexity of the resulting expressions that arise from (49), below we only write down the general form of the equation for the critical separations (h_c) as

$$\sum_{i=0}^4 a_i \left(\frac{h_c}{z_0} \right)^{n_i} = 0, \quad (53)$$

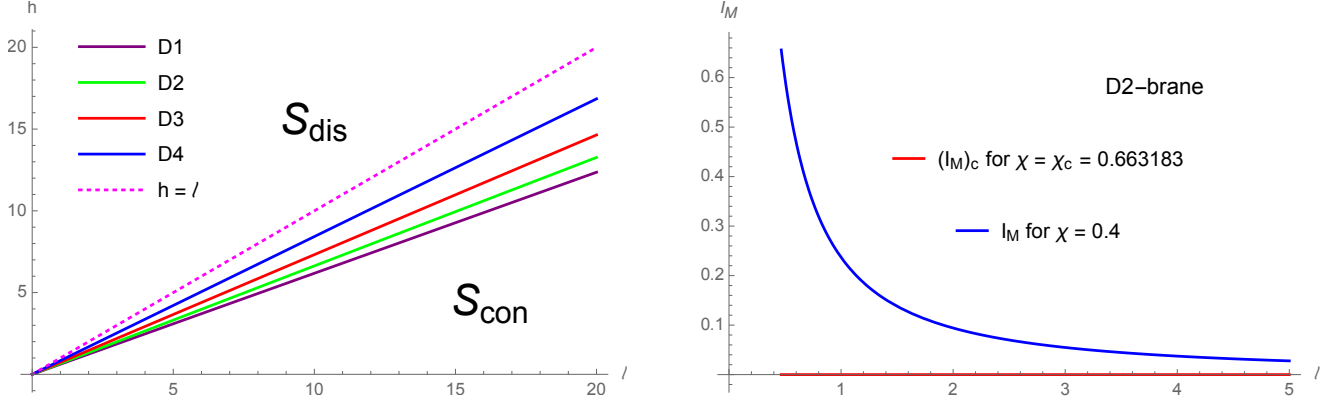


Figure 5: **A:** The phase diagrams corresponding to different Dp -branes. The entire region above an individual curve corresponds to the disconnected phase (S_{dis}), while that below an individual curve corresponds to the connected phase (S_{con}). The dotted line corresponds to $h = \ell$. **B:** Mutual information (I_M) *versus* strip width (ℓ) plot for D2-brane.

where we have used results from section 3.1. In (53), the numerical coefficients a_i are certain combinations of gamma functions whose explicit expressions can be written in terms of various constants that appear in section 3.1 and Θ in (38) and are presented in table A in appendix A. On the other hand, the exponents n_i may be given as⁹

$$\begin{aligned}
\text{for D1-brane:} & \quad (n_0 = 0, n_1 = 1, n_2 = 2, n_3 = 3, n_4 = 6), \\
\text{for D2-brane:} & \quad \left(n_0 = 0, n_1 = \frac{4}{3}, n_2 = \frac{7}{3}, n_3 = \frac{10}{3}, n_4 = \frac{20}{3} \right), \\
\text{for D3-brane:} & \quad (n_0 = 0, n_1 = 2, n_2 = 3, n_3 = 4, n_4 = 8), \\
\text{for D4-brane:} & \quad (n_0 = 0, n_1 = 4, n_2 = 5, n_3 = 6, n_4 = 12).
\end{aligned} \tag{54}$$

Finally, we explicitly check the inequality (1) by numerically plotting both E_W and $I_M(A, B)/2$ against the dimensionless quantity hT in fig.6. Note that, in plotting fig.6 we have used (37) and (48). In addition to validate (1), these plots also show the monotonically decreasing nature of both E_W and $I_M(A, B)$. Moreover, beyond the critical separation $h_c T$ ($T = 1$) determined by (53) both of them approach zero which is an essential nature for the phase transition discussed above [9, 11, 13, 14, 15].

4 Conclusions

In this paper, we have studied aspects of holographic entanglement measures for certain class of non-conformal field theories which are holographic dual to non-conformal Dp -brane backgrounds [28, 29, 30, 31, 32]. Within the framework of the Gauge/Gravity duality, we explicitly computed entanglement wedge cross section (EWCS), holographic entanglement entropy (HEE) and holographic mutual information (HMI) for these field theories. In our analysis, we considered $p = 1, 2, 4$; while $p = 3$ corresponds to the usual $\text{AdS}_5/\text{CFT}_4$ duality [1]. In our computations, we considered a bipartite system with two parallel entangling regions of equal width ℓ and length L separated by a

⁹The corresponding expression for D3-brane may be compared with that already available in the literature; see, e.g., [20, 21].

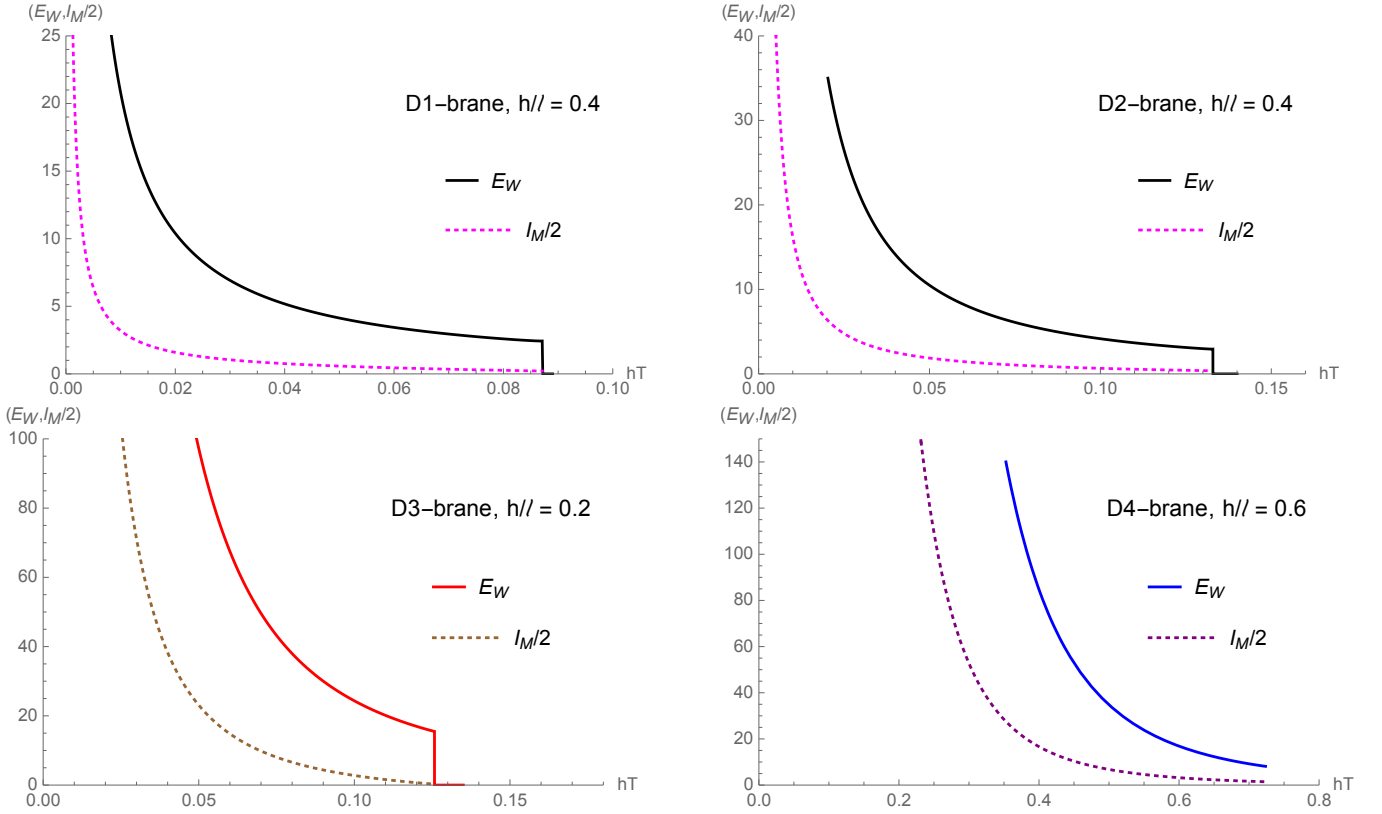


Figure 6: Holographic Mutual Information ($I_M/2$) plots for different non-conformal backgrounds.

Notice that, in all the cases $E_W \geq I_M/2$. We set $\frac{L^{p-1}}{4G_N^{p+2}} \frac{(g_{YM}^2 N)^{\frac{(p-3)}{(5-p)}}}{\Delta^{\frac{p-1}{5-p}}} = 1$

distance h . Implementing analytical as well as numerical methods, we observe that the qualitative behaviours of the above mentioned holographic measures are similar to those of the conformal case: both the EWCS and HMI show monotonically decreasing behaviour with temperature. However, while the previous one discontinuously drops down to zero value beyond a critical separation distance h_c between the entangling subregions, the later attains zero value at h_c in a smooth and continuous fashion. This suggests a first order phase transition between connected and disconnected phases of the bipartite system. In our analysis, we have also been able to compute this critical values analytically. Our analysis indeed establishes the fact that the qualitative behaviours of the holographic information quantities are similar irrespective of whether the boundary field theory is conformal or not.

We believe that this non trivial analysis of information quantities, in the light of Gauge/Gravity correspondence, will be extremely useful in order to understand aspects of field theories with explicit breaking of conformal invariance. From this point of view, it seems fascinating to consider quantum corrections to both EWCS and HEE in these holographic set-ups [8]. On top of that, other relevant measures, such as, entanglement negativity [16], reflected entropy [17, 18], etc., can also be studied within these non-conformal theories. It will be equally interesting to study the evolution and scaling of EWCS after thermal as well as electromagnetic quenches [25, 26, 27] corresponding to these theories. These we plan to explore in future.

Acknowledgments

The present work is supported by the Chilean *National Agency for Research and Development* (ANID)/ FONDECYT / POSTDOCTORADO BECAS CHILE / Project No. 3190021. I would like to thank Shankhadeep Chakraborty, Suvankar Dutta, Radouane Gannouji, M. Reza Mohammadi Mozaffar and especially Karunava Sil for very useful discussions. I would also like to thank the referee for her/his valuable comments.

Dedication: This article is dedicated to the memory of Mr. Anup Lala.

A Various coefficients appearing in section (3.1)

The coefficients appearing in (28) [D1-brane] are given by

$$\begin{aligned}\mathcal{C}_1 &= \frac{\pi \Gamma\left(\frac{-1}{4}\right) \Gamma\left(\frac{3}{4}\right)}{16 \Gamma\left(\frac{1}{4}\right) \Gamma\left(\frac{5}{4}\right)}, \\ \mathcal{C}_2 &= \frac{1}{\mathcal{C}_1} \frac{16 \Gamma\left(\frac{5}{4}\right)^2}{\Gamma\left(\frac{3}{4}\right)^2} \left(1 + \frac{\Gamma\left(\frac{-1}{4}\right) \Gamma\left(\frac{5}{4}\right)}{2 \Gamma\left(\frac{1}{4}\right) \Gamma\left(\frac{3}{4}\right)}\right), \\ \mathcal{C}_3 &= \frac{1}{\mathcal{C}_1} \frac{4096 \Gamma\left(\frac{5}{4}\right)^6}{\pi \Gamma\left(\frac{3}{4}\right)^6} \left[\frac{4 \Gamma\left(\frac{3}{4}\right)}{5 \pi^{3/2}} + \frac{3 \Gamma\left(\frac{9}{4}\right) \Gamma\left(\frac{-1}{4}\right)}{2 \pi \Gamma\left(\frac{1}{4}\right) \Gamma\left(\frac{11}{4}\right)} - 1\right].\end{aligned}\tag{A.1}$$

The coefficients appearing in (30) [D2-brane] are written as

$$\begin{aligned}\mathcal{D}_1 &= \frac{2^{8/3} \pi^{7/6} \Gamma\left(\frac{-2}{7}\right)}{49 \sqrt[3]{21} \Gamma\left(\frac{3}{14}\right)} \left(\frac{\Gamma\left(\frac{5}{7}\right)}{\Gamma\left(\frac{17}{14}\right)}\right)^{4/3}, \\ \mathcal{D}_2 &= \frac{1}{\mathcal{D}_1} \frac{63 \Gamma\left(\frac{17}{14}\right)^3}{8 \sqrt{\pi} \Gamma\left(\frac{5}{7}\right)^3} \left[\frac{\Gamma\left(\frac{-2}{7}\right) \Gamma\left(\frac{10}{7}\right)}{\Gamma\left(\frac{3}{14}\right) \Gamma\left(\frac{27}{14}\right)} + \frac{3 \Gamma\left(\frac{3}{7}\right) \Gamma\left(\frac{5}{7}\right)}{\Gamma\left(\frac{17}{14}\right) \Gamma\left(\frac{13}{14}\right)}\right], \\ \mathcal{D}_3 &= \frac{1}{\mathcal{D}_1} \left[-\frac{1750329 \sqrt[3]{21} \Gamma\left(\frac{3}{7}\right) \Gamma\left(\frac{17}{14}\right)^{19/3} \Gamma\left(\frac{10}{7}\right)}{2048 \cdot 2^{2/3} \pi^{13/6} \Gamma\left(\frac{5}{7}\right)^{19/3} \Gamma\left(\frac{13}{14}\right) \Gamma\left(\frac{27}{14}\right)} \right. \\ &\quad + \frac{2^{2/3} \pi^{7/6} \Gamma\left(\frac{-2}{7}\right)}{245 \sqrt[3]{21} \Gamma\left(\frac{3}{14}\right)} \left(\frac{\Gamma\left(\frac{5}{7}\right)}{\Gamma\left(\frac{17}{14}\right)}\right)^{4/3} \left(\frac{333534915 \cdot 21^{2/3} \Gamma\left(\frac{17}{14}\right)^{26/3} \Gamma\left(\frac{10}{7}\right)^2}{4096 \sqrt[3]{2} \pi^{10/3} \Gamma\left(\frac{5}{7}\right)^{26/3} \Gamma\left(\frac{27}{14}\right)^2}\right. \\ &\quad \left. + \frac{142943535 \cdot 21^{2/3} \Gamma\left(\frac{17}{14}\right)^{20/3} \left(3 \Gamma\left(\frac{5}{7}\right) \Gamma\left(\frac{17}{14}\right) \Gamma\left(\frac{27}{14}\right)^2 \Gamma\left(\frac{15}{7}\right) - 2 \Gamma\left(\frac{17}{14}\right)^2 \Gamma\left(\frac{10}{7}\right)^2 \Gamma\left(\frac{37}{14}\right)\right)}{4096 \sqrt[3]{2} \pi^{10/3} \Gamma\left(\frac{5}{7}\right)^{26/3} \Gamma\left(\frac{27}{14}\right)^2 \Gamma\left(\frac{37}{14}\right)}\right) + \\ &\quad \left. \frac{5250987 \sqrt[3]{21} \Gamma\left(\frac{8}{7}\right) \Gamma\left(\frac{17}{14}\right)^{16/3}}{8192 \cdot 2^{2/3} \pi^{13/6} \Gamma\left(\frac{5}{7}\right)^{16/3} \Gamma\left(\frac{23}{7}\right)}\right].\end{aligned}\tag{A.2}$$

The coefficients in (32) [D3-brane] are of the following forms:

$$\begin{aligned}
\mathcal{B}_1 &= \frac{\pi^{3/2} \Gamma\left(-\frac{1}{3}\right) \Gamma\left(\frac{2}{3}\right)^2}{27 \Gamma\left(\frac{1}{6}\right) \Gamma\left(\frac{7}{6}\right)^2}, \\
\mathcal{B}_2 &= \frac{1}{\mathcal{B}_1} \left(\frac{3 \Gamma\left(\frac{4}{3}\right) \Gamma\left(-\frac{1}{3}\right) \Gamma\left(\frac{7}{6}\right)^3}{\sqrt{\pi} \Gamma\left(\frac{1}{6}\right) \Gamma\left(\frac{2}{3}\right)^3 \Gamma\left(\frac{11}{6}\right)} + \frac{3 \Gamma\left(\frac{1}{3}\right) \Gamma\left(\frac{7}{6}\right)^2}{2 \sqrt{\pi} \Gamma\left(\frac{2}{3}\right)^2 \Gamma\left(\frac{5}{6}\right)} \right), \\
\mathcal{B}_3 &= \frac{1}{\mathcal{B}_1} \left[\frac{243 \Gamma\left(\frac{7}{6}\right)^7}{2 \pi^{5/2} \Gamma\left(\frac{2}{3}\right)^7} \left(\frac{3 \Gamma\left(\frac{2}{3}\right)}{8 \Gamma\left(\frac{7}{6}\right)} - \frac{\Gamma\left(\frac{1}{3}\right) \Gamma\left(\frac{4}{3}\right)}{\Gamma\left(\frac{5}{6}\right) \Gamma\left(\frac{11}{6}\right)} \right) + \right. \\
&\quad \left. \frac{\pi^{3/2} \Gamma\left(-\frac{1}{3}\right) \Gamma\left(\frac{2}{3}\right)^2 \left(\frac{39366 \Gamma\left(\frac{7}{6}\right)^{10} \Gamma\left(\frac{4}{3}\right)^2}{\pi^4 \Gamma\left(\frac{2}{3}\right)^{10} \Gamma\left(\frac{11}{6}\right)^2} - \frac{26244 \Gamma\left(\frac{7}{6}\right)^9 \left(\sqrt{\pi} \Gamma\left(\frac{7}{6}\right) \Gamma\left(\frac{4}{3}\right)^2 - 2 \Gamma\left(\frac{2}{3}\right) \Gamma\left(\frac{11}{6}\right)^2 \right)}{\pi^{9/2} \Gamma\left(\frac{2}{3}\right)^{10} \Gamma\left(\frac{11}{6}\right)^2} \right)}{216 \Gamma\left(\frac{1}{6}\right) \Gamma\left(\frac{7}{6}\right)^2} \right]. \quad (\text{A.3})
\end{aligned}$$

Finally, the coefficients in (34) [D4-brane] are written as

$$\begin{aligned}
\mathcal{E}_1 &= \frac{256 \pi^{5/2} \Gamma\left(-\frac{2}{5}\right) \Gamma\left(\frac{3}{5}\right)^4}{3125 \Gamma\left(\frac{1}{10}\right) \Gamma\left(\frac{11}{10}\right)^4}, \\
\mathcal{E}_2 &= \frac{1}{\mathcal{E}_1} \frac{5 \Gamma\left(\frac{11}{10}\right)^3}{8 \sqrt{\pi} \Gamma\left(\frac{3}{5}\right)^3} \left(\frac{\Gamma\left(-\frac{2}{5}\right) \Gamma\left(\frac{6}{5}\right)}{\Gamma\left(\frac{1}{10}\right) \Gamma\left(\frac{17}{10}\right)} + \frac{\Gamma\left(\frac{1}{5}\right) \Gamma\left(\frac{3}{5}\right)}{4 \Gamma\left(\frac{7}{10}\right) \Gamma\left(\frac{11}{10}\right)} \right), \\
\mathcal{E}_3 &= \frac{1}{\mathcal{E}_1} \left[- \frac{78125 \Gamma\left(\frac{1}{5}\right) \Gamma\left(\frac{11}{10}\right)^9 \Gamma\left(\frac{6}{5}\right)}{131072 \pi^{7/2} \Gamma\left(\frac{3}{5}\right)^9 \Gamma\left(\frac{7}{10}\right) \Gamma\left(\frac{17}{10}\right)} + \frac{234375 \Gamma\left(\frac{4}{5}\right) \Gamma\left(\frac{11}{10}\right)^8}{524288 \pi^{7/2} \Gamma\left(\frac{3}{5}\right)^8 \Gamma\left(\frac{13}{5}\right)} + \right. \\
&\quad \left. \frac{64 \pi^{5/2} \Gamma\left(-\frac{2}{5}\right) \Gamma\left(\frac{3}{5}\right)^4 \left(\frac{3662109375 \Gamma\left(\frac{6}{5}\right)^2 \Gamma\left(\frac{11}{10}\right)^{14}}{8388608 \pi^6 \Gamma\left(\frac{3}{5}\right)^{14} \Gamma\left(\frac{17}{10}\right)^2} + \frac{732421875 \left(3 \Gamma\left(\frac{3}{5}\right) \Gamma\left(\frac{17}{10}\right)^2 \Gamma\left(\frac{9}{5}\right) - 2 \Gamma\left(\frac{11}{10}\right) \Gamma\left(\frac{6}{5}\right)^2 \Gamma\left(\frac{23}{10}\right) \right) \Gamma\left(\frac{11}{10}\right)^{13}}{8388608 \pi^6 \Gamma\left(\frac{3}{5}\right)^{14} \Gamma\left(\frac{17}{10}\right)^2 \Gamma\left(\frac{23}{10}\right)} \right)}{9375 \Gamma\left(\frac{1}{10}\right) \Gamma\left(\frac{11}{10}\right)^4} \right]. \quad (\text{A.4})
\end{aligned}$$

The coefficients a_i in (53) can be expressed in terms of the constants appearing in (A.1)-(A.4) as follows:

Background	a_0	a_1	a_2	a_3	a_4
D1	\mathcal{C}_1	$-\Theta_{p=1}/2$	2	$\mathcal{C}_1 \mathcal{C}_2$	$\mathcal{C}_1 \mathcal{C}_3$
D2	\mathcal{D}_1	$-\Theta_{p=2}/2$	9/8	$\mathcal{D}_1 \mathcal{D}_2$	$\mathcal{D}_1 \mathcal{D}_3$
D3	\mathcal{B}_1	$-\Theta_{p=3}/2$	1/2	$\mathcal{B}_1 \mathcal{B}_2$	$\mathcal{B}_1 \mathcal{B}_3$
D4	\mathcal{E}_1	$-\Theta_{p=4}/2$	1/8	$\mathcal{E}_1 \mathcal{E}_2$	$\mathcal{E}_1 \mathcal{E}_3$

Table 1: Values of the coefficients a_i in (53) corresponding to different background configurations. Here $\Theta_{p=\#}$ corresponds to the value of the coefficient Θ in (38) for different values of $p(= 1, 2, 3, 4)$.

References

- [1] J. M. Maldacena, “The Large N limit of superconformal field theories and supergravity,” *Int. J. Theor. Phys.* **38** (1999), 1113-1133, *Adv. Theor. Math. Phys.* **2** (1998) 231-252, doi:10.1023/A:1026654312961 [arXiv:hep-th/9711200 [hep-th]].
- [2] E. Witten, “Anti-de Sitter space and holography,” *Adv. Theor. Math. Phys.* **2** (1998), 253-291 doi:10.4310/ATMP.1998.v2.n2.a2 [arXiv:hep-th/9802150 [hep-th]].
- [3] O. Aharony, S. S. Gubser, J. M. Maldacena, H. Ooguri and Y. Oz, “Large N field theories, string theory and gravity,” *Phys. Rept.* **323** (2000), 183-386 doi:10.1016/S0370-1573(99)00083-6 [arXiv:hep-th/9905111 [hep-th]].
- [4] S. Ryu and T. Takayanagi, “Holographic derivation of entanglement entropy from AdS/CFT,” *Phys. Rev. Lett.* **96** (2006), 181602 doi:10.1103/PhysRevLett.96.181602 [arXiv:hep-th/0603001 [hep-th]].
- [5] S. Ryu and T. Takayanagi, “Aspects of Holographic Entanglement Entropy,” *JHEP* **08** (2006), 045 doi:10.1088/1126-6708/2006/08/045 [arXiv:hep-th/0605073 [hep-th]].
- [6] V. E. Hubeny, M. Rangamani and T. Takayanagi, “A Covariant holographic entanglement entropy proposal,” *JHEP* **07** (2007), 062 doi:10.1088/1126-6708/2007/07/062 [arXiv:0705.0016 [hep-th]].
- [7] H. Casini, M. Huerta and R. C. Myers, “Towards a derivation of holographic entanglement entropy,” *JHEP* **05** (2011), 036 doi:10.1007/JHEP05(2011)036 [arXiv:1102.0440 [hep-th]].
- [8] T. Faulkner, A. Lewkowycz and J. Maldacena, “Quantum corrections to holographic entanglement entropy,” *JHEP* **11** (2013), 074 doi:10.1007/JHEP11(2013)074 [arXiv:1307.2892 [hep-th]].
- [9] O. Ben-Ami, D. Carmi and J. Sonnenschein, “Holographic Entanglement Entropy of Multiple Strips,” *JHEP* **11** (2014), 144 doi:10.1007/JHEP11(2014)144 [arXiv:1409.6305 [hep-th]].
- [10] M. M. Wolf, F. Verstraete, M. B. Hastings and J. I. Cirac, “Area Laws in Quantum Systems: Mutual Information and Correlations,” *Phys. Rev. Lett.* **100** (2008) no.7, 070502 doi:10.1103/PhysRevLett.100.070502 [arXiv:0704.3906 [quant-ph]].
- [11] M. Headrick, “Entanglement Renyi entropies in holographic theories,” *Phys. Rev. D* **82** (2010), 126010 doi:10.1103/PhysRevD.82.126010 [arXiv:1006.0047 [hep-th]].
- [12] W. Fischler, A. Kundu and S. Kundu, “Holographic Mutual Information at Finite Temperature,” *Phys. Rev. D* **87** (2013) no.12, 126012 doi:10.1103/PhysRevD.87.126012 [arXiv:1212.4764 [hep-th]].
- [13] T. Takayanagi and K. Umemoto, “Entanglement of purification through holographic duality,” *Nature Phys.* **14** (2018) no.6, 573-577 doi:10.1038/s41567-018-0075-2 [arXiv:1708.09393 [hep-th]].
- [14] P. Nguyen, T. Devakul, M. G. Halbasch, M. P. Zaletel and B. Swingle, “Entanglement of purification: from spin chains to holography,” *JHEP* **01** (2018), 098 doi:10.1007/JHEP01(2018)098 [arXiv:1709.07424 [hep-th]].

- [15] B. M. Terhal, M. Horodecki, D. W. Leung and D. P. DiVincenzo, “The entanglement of purification,” *J. Math. Phys.* **43** (2002) 4286 [quan-ph/0202044].
- [16] J. Kudler-Flam and S. Ryu, “Entanglement negativity and minimal entanglement wedge cross sections in holographic theories,” *Phys. Rev. D* **99** (2019) no.10, 106014 doi:10.1103/PhysRevD.99.106014 [arXiv:1808.00446 [hep-th]].
- [17] S. Dutta and T. Faulkner, “A canonical purification for the entanglement wedge cross-section,” [arXiv:1905.00577 [hep-th]].
- [18] H. S. Jeong, K. Y. Kim and M. Nishida, “Reflected Entropy and Entanglement Wedge Cross Section with the First Order Correction,” *JHEP* **12** (2019), 170 doi:10.1007/JHEP12(2019)170 [arXiv:1909.02806 [hep-th]].
- [19] K. Babaei Velni, M. R. Mohammadi Mozaffar and M. H. Vahidinia, “Some Aspects of Entanglement Wedge Cross-Section,” *JHEP* **05** (2019), 200 doi:10.1007/JHEP05(2019)200 [arXiv:1903.08490 [hep-th]].
- [20] N. Jokela and A. Pönni, “Notes on entanglement wedge cross sections,” *JHEP* **07** (2019), 087 doi:10.1007/JHEP07(2019)087 [arXiv:1904.09582 [hep-th]].
- [21] S. Chakraborty, S. Pant and K. Sil, “Effect of back reaction on entanglement and subregion volume complexity in strongly coupled plasma,” *JHEP* **06** (2020), 061 doi:10.1007/JHEP06(2020)061 [arXiv:2004.06991 [hep-th]].
- [22] Y. f. Huang, Z. j. Shi, C. Niu, C. y. Zhang and P. Liu, “Mixed State Entanglement for Holographic Axion Model,” *Eur. Phys. J. C* **80** (2020) no.5, 426 doi:10.1140/epjc/s10052-020-7921-y [arXiv:1911.10977 [hep-th]].
- [23] J. Boruch, “Entanglement wedge cross-section in shock wave geometries,” *JHEP* **07** (2020), 208 doi:10.1007/JHEP07(2020)208 [arXiv:2006.10625 [hep-th]].
- [24] G. Fu, P. Liu, H. Gong, X. M. Kuang and J. P. Wu, “Informational properties for Einstein-Maxwell-Dilaton Gravity,” [arXiv:2007.06001 [hep-th]].
- [25] R. Q. Yang, C. Y. Zhang and W. M. Li, “Holographic entanglement of purification for thermofield double states and thermal quench,” *JHEP* **01** (2019), 114 doi:10.1007/JHEP01(2019)114 [arXiv:1810.00420 [hep-th]].
- [26] J. Kudler-Flam, Y. Kusuki and S. Ryu, “Correlation measures and the entanglement wedge cross-section after quantum quenches in two-dimensional conformal field theories,” *JHEP* **04** (2020), 074 doi:10.1007/JHEP04(2020)074 [arXiv:2001.05501 [hep-th]].
- [27] K. Babaei Velni, M. R. Mohammadi Mozaffar and M. H. Vahidinia, “Evolution of entanglement wedge cross section following a global quench,” *JHEP* **08** (2020), 129 doi:10.1007/JHEP08(2020)129 [arXiv:2005.05673 [hep-th]].
- [28] N. Izhaki, J. M. Maldacena, J. Sonnenschein and S. Yankielowicz, “Supergravity and the large N limit of theories with sixteen supercharges,” *Phys. Rev. D* **58** (1998), 046004 doi:10.1103/PhysRevD.58.046004 [arXiv:hep-th/9802042 [hep-th]].

- [29] H. J. Boonstra, K. Skenderis and P. K. Townsend, “The domain wall / QFT correspondence,” JHEP **01** (1999), 003 doi:10.1088/1126-6708/1999/01/003 [arXiv:hep-th/9807137 [hep-th]].
K. Skenderis, “Field theory limit of branes and gauged supergravities,” Fortsch. Phys. **48** (2000), 205-208 doi:10.1002/(SICI)1521-3978(20001)48:1/3;205::AID-PROP205;3.0.CO;2-F [arXiv:hep-th/9903003 [hep-th]].
- [30] I. Kanitscheider, K. Skenderis and M. Taylor, “Precision holography for non-conformal branes,” JHEP **09** (2008), 094 doi:10.1088/1126-6708/2008/09/094 [arXiv:0807.3324 [hep-th]].
- [31] D. W. Pang, “Entanglement thermodynamics for nonconformal D-branes,” Phys. Rev. D **88** (2013) no.12, 126001 doi:10.1103/PhysRevD.88.126001 [arXiv:1310.3676 [hep-th]].
- [32] D. W. Pang, “Corner contributions to holographic entanglement entropy in non-conformal backgrounds,” JHEP **09** (2015), 133 doi:10.1007/JHEP09(2015)133 [arXiv:1506.07979 [hep-th]].
- [33] K. Narayan, “On Lifshitz scaling and hyperscaling violation in string theory,” Phys. Rev. D **85** (2012), 106006 doi:10.1103/PhysRevD.85.106006 [arXiv:1202.5935 [hep-th]].
- [34] H. Singh, “Lifshitz/Schrödinger Dp-branes and dynamical exponents,” JHEP **07** (2012), 082 doi:10.1007/JHEP07(2012)082 [arXiv:1202.6533 [hep-th]].
- [35] K. Narayan, “Non-conformal brane plane waves and entanglement entropy,” Phys. Lett. B **726** (2013), 370-374 doi:10.1016/j.physletb.2013.07.061 [arXiv:1304.6697 [hep-th]].
- [36] R. Mishra and H. Singh, “Entanglement asymmetry for boosted black branes and the bound,” Int. J. Mod. Phys. A **32** (2017) no.16, 1750091 doi:10.1142/S0217751X17500919 [arXiv:1603.06058 [hep-th]].
- [37] A. van Niekerk, “Entanglement Entropy in NonConformal Holographic Theories,” [arXiv:1108.2294 [hep-th]].
- [38] W. Fischler and S. Kundu, “Strongly Coupled Gauge Theories: High and Low Temperature Behavior of Non-local Observables,” JHEP **05** (2013), 098 doi:10.1007/JHEP05(2013)098 [arXiv:1212.2643 [hep-th]].
- [39] S. Kundu and J. F. Pedraza, “Aspects of Holographic Entanglement at Finite Temperature and Chemical Potential,” JHEP **08** (2016), 177 doi:10.1007/JHEP08(2016)177 [arXiv:1602.07353 [hep-th]].
- [40] Robert M. Wald, General relativity, Chicago Univ. Press, Chicago, IL, 1984.